Electron Track Reconstruction and Improved Modulation for Photoelectric X-ray Polarimetry

Tenglin Li [a,b], Ming Zeng [a,b *], Hua Feng [a,b,c], Jirong Cang [a,b], Hong Li [a,b,c], Heng Zhang [a,b,c], Zhi Zeng [a,b] , Jianping Cheng [a,b], Hao Ma [a,b], Yinong Liu [a,b]

[a] *Department of Engineering Physics, Tsinghua University, Beijing 100084, China*

[b] *Key Laboratory of Particle & Radiation Imaging (Tsinghua University), Ministry of Education, China*

[c] *Center for Astrophysics, Tsinghua University, Beijing 100084, China*

Abstract

The key to photoelectric X-ray polarimetry is the determination of the emission direction of photoelectrons. Due to the low mass of an electron, the ionization trajectory is not straight and the useful information needed for polarization is stored only in the initial part of the track where less energy is deposited. We present a new algorithm, based on the shortest path problem in graph theory, to reconstruct the 2D electron track from the measured image that is blurred due to transversal diffusion along drift and multiplication in the gas chamber. Compared with previous methods based on moment analysis, this algorithm allows us to identify the photoelectric interaction point more accurately and precisely than previous, especially for complicated tracks resulted from high energy photons or low pressure chambers. This leads to a higher degree of modulation and consequently a better sensitivity toward high energy X-rays. The new algorithm is justified using simulations and measurements with the gas pixel detector but it should also work for other polarimetric techniques such as the time projection chamber.

Keywords: X-ray, Polarimetry, Astrophysics, Track Reconstruction

1 Introduction

Sensitive X-ray polarimetry on the basis of the photoelectric effect has become possible in recent years with the development of high-resolution micro-pattern gas detectors [1, 2]. The azimuthal distribution of the photoelectron direction is dependent on the polarization of the X-ray. The goal of these gas polarimeters is to measure the 2D photoelectron directions on the plane perpendicular to the incident X-rays. The sensitivity of the polarimeter depends on how accurate and precise the direction can be measured. Thus, the algorithm to reconstruct the photoelectron emission direction from the measured track image is essential.

Previously, the reconstruction for the electron emission direction was fulfilled based on the moment analysis of the track image [3, 4]. First, the barycentre and the principal axis (second moment) of the entire charge deposition are calculated. The third moment is then computed to determine which side along the principle axis contains the interaction point (less charge) and which one is the end point or the Bragg peak (more charge). Then, the most important step is to locate the interaction point by selecting pixels around it (between a smaller and a larger radius

* Corresponding author, *E-mail*: zengming@tsinghua.edu.cn

from the barycentre) and calculating their barycentre. Once the interaction point is found, the emission angle can be derived as the principle axis of a distance-weighted change map around it.

How the interaction point can be located accurately and precisely is the most important and challenge part for direction reconstruction. However, the above algorithm may fail for complicated tracks, as it simplifies the track image into elliptical distributions of charges. For example, if the photoelectron moves back and forth and stops not at the very end, the algorithm may misidentify the location of the interaction point. For the gas pixel detector (GPD) filled with 0.8 atm dimethyl ether (DME) [1, 5], the current algorithm produces reasonable modulations at energies below ~7 keV, but is not optimal at energies above due to complication of the electron tracks. The situation may be even worse for the time projection polarimeter [2], as it is filled with low pressure (0.25 atm) gas.

In this paper, we propose a new algorithm to locate the interaction point via reconstruction of the full electron track. The algorithm is described in Section 2. The results tested with simulated and measured data with the GPD polarimeter are discussed in Section 3. The conclusion is summarized in Section 4.

2 The track reconstruction algorithm

In the following of the paper, the algorithm is demonstrated and tested with simulated and measured data given the GPD polarimeter, for which the detector structure and configuration can be found from Ref. [5]. The image has hexagonal pixels with a pitch of 50 μm and the full width at half maximum (FWHM) for the total transversal diffusion is on the order of 150 μm.

2.1 Track reconstruction

We take a simulated event generated by a 15 keV X-ray photon to illustrate the track reconstruction algorithm. The photon deposits all of its energy by photoelectric effect, and the photoelectron leaves behind a track of charge via ionization (see Fig. 1a for a 2D projection of the track on the readout plane, simulated using GEANT4). Secondary electrons created by the photoelectron will drift along the electric field toward the readout plane and get multiplied when they go through the gas electron multiplier (GEM). This process will introduce transversal diffusion and dilute the charge image by a factor of σ_{drift} and σ_{multi}, respectively. The value of σ_{drift} is distance dependent while σ_{multi} is fixed; both are taken into account in the simulation. The electrons are then accumulated on the hexagonal pixels of the readout chip when they approach the detector plane, on top of the readout noise (Fig. 1b). Our simulation package can produce well consistent images and statistical results with real measurements [5], justifying the use of simulations for the test of the new algorithm in this paper.

Due to the presence of a noise cut, the measured charge distribution (image) may be broken into several disconnected segments (or clusters of points). The example illustrated in Fig. 1c consists of three individual clusters, denoted as A, B, and C. The *clustering algorithm* is used to identify individual clusters and the neighbouring ones are connected with each other via their nearest pixels if closer than a certain threshold (0.25 mm in this case). Clusters less than 10 pixels are discarded as they may be caused by noise or other effects such as absorption of re-emitted characteristic X-rays in the gas. Then the 2D image can be used for track reconstruction, following the steps described below.

1. **Connecting points** (Fig. 1c). In the graph theory, the *points* are mathematical abstractions for the interconnected objects and the *lines* describe the connectivity between the points. In this paper, points are defined as the pixelated energy depositions and two points are connected with a line if they are next to each other (i.e., the space between two points equals 50 μm).
2. **Calculating the primary path** (Fig. 1d). According to the shortest path problems in graph theory [6], we can calculate the *shortest path* given by any two points in the graph. The length of a path in this paper is defined as the actual spatial length of it. Among all of the shortest paths between every two points, we select the longest one, defined as the *primary path*, which is a rough estimate of the track (see Fig. 1d). If the longest path is not unique, the one with the minimum deflection is selected.
3. **Spatial filtering and track reconstruction** (Fig. 1e). The primary path found above often traces the edge of the track pixels. To make it trace the centroid of the track, we apply a spatial energy filter to smooth the polyline: every point in the primary path is replaced by the charge barycentre within a certain radius around it. Thus a new track (called *reconstructed path*, see Fig. 1e) is obtained, which is smoother and closer to the center of the ionization track than the primary path. The filter radius (0.22 mm in our case) is related to the size of the total transversal diffusion, to match the actual width of the track. By calculating the sum of charge deposition around each endpoint of the reconstructed path, we can determine which one is the photoelectric interaction point (less charge) and which one is the Bragg peak (more charge).

After these steps, the reconstructed path and interaction point are obtained. The comparison between the reconstructed path and original ionization track is shown in Fig. 1f. It is obvious that the new algorithm can provide a reasonable reconstruction for the track and an accurate and precise estimate of the interaction point.

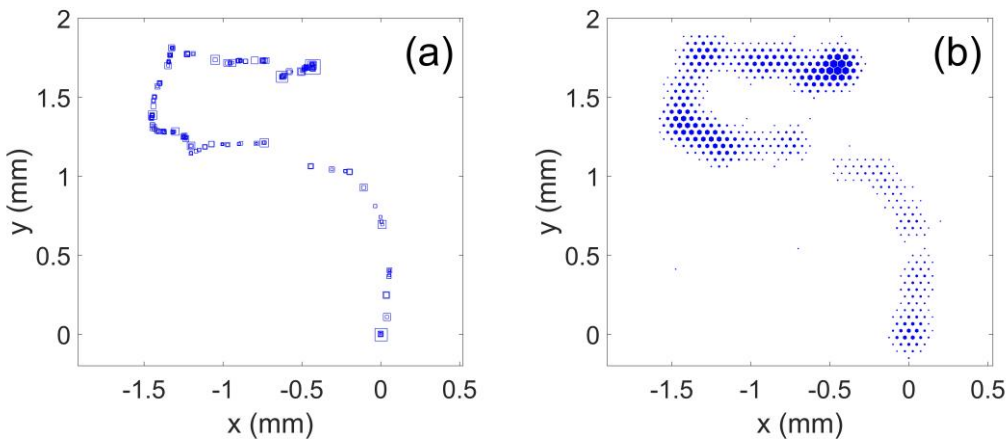

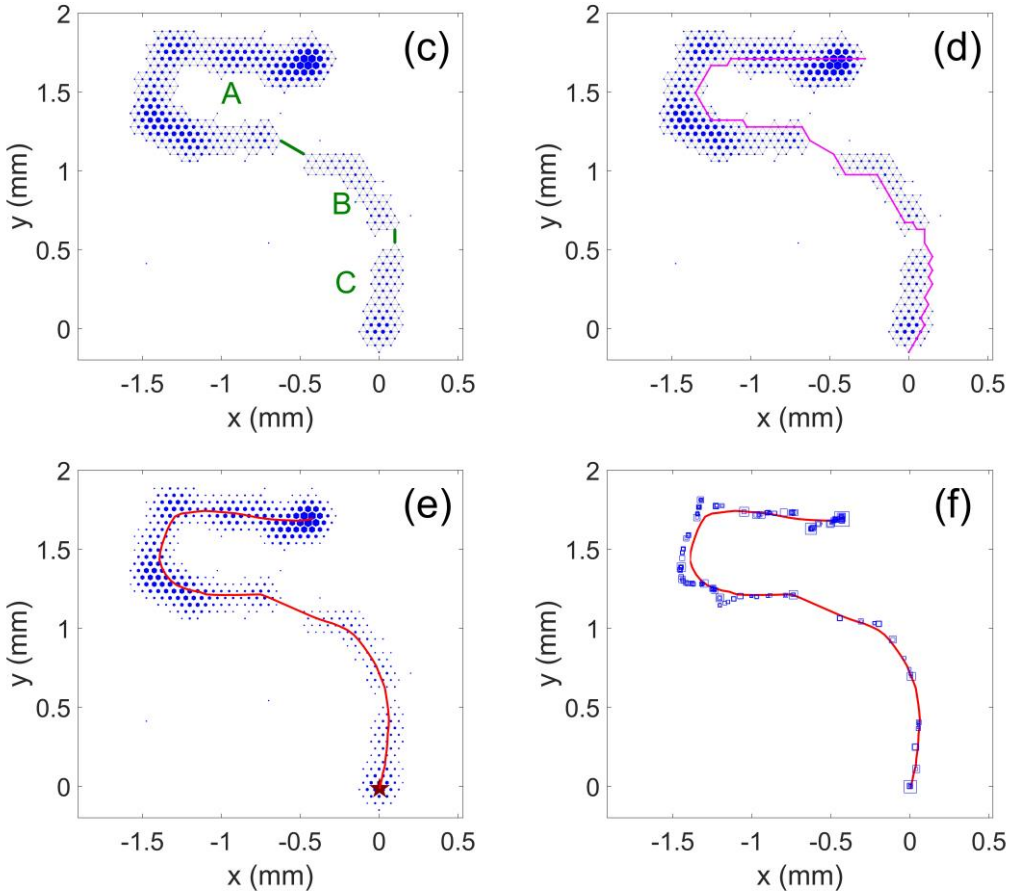

Fig. 1. Illustration of the track reconstruction algorithm. **(a)** Simulated charge distribution produced by a 15 keV X-ray projected onto the plane perpendicular to the X-ray direction. The sizes of the markers are proportional to the value of the energy deposition (similarly hereafter). **(b)** Image obtained by the readout ASIC of the GPD detector. **(c)** Neighbouring clusters and neighbouring points are connected (green and black lines, respectively). **(d)** For all shortest paths between every two points in the graph, the longest one is defined as the primary path (magenta line). **(e)** The reconstructed path (red line) is derived from primary path after a spatial energy filtering. The end with less charge depositions is determined as the interaction point (red star). **(f)** Comparison of the reconstructed path and the initial charge distribution.

2.2 **Emission angle reconstruction**

Once the interaction point is estimated, the 2D emission direction of the photoelectron is calculated as the principle axis of a distance-weighted map around the interaction point. Adopted from Ref. [4], the weight $W(d_{\mathrm{ip}})$ is defined as:

$$W(d_{\mathrm{ip}}) = \exp(-d_{\mathrm{ip}} / w) ,$$

Where w is a constant derived from Monte Carlo simulations (0.05 mm in this case) and d_{ip} is the distance from each pixel to the estimated interaction point.

Then the emission angle can be computed as the direction of the second moment of the entire weighted map.

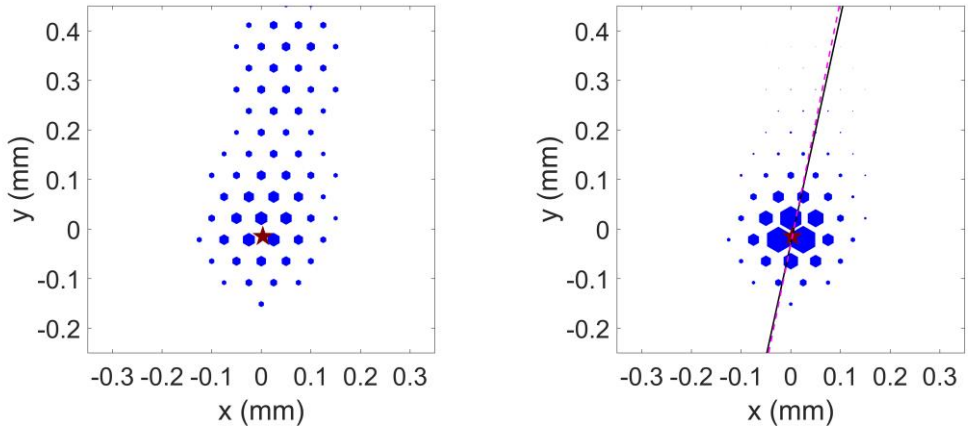

Fig. 2. The detected map (left) and weighted map (right) around the reconstructed interaction point (red star). The reconstructed emission direction (dashed) approximates the true emission direction (solid).

3 Results and Discussion

Following previous algorithms, we only search for the interaction point via track reconstruction for track images that have an eccentricity larger than 2. For those of small eccentricity, the principal axis of the entire image is adopted as the estimate of the emission direction. This fraction (eccentricity less than 2) ranges from ~26% at 5 keV, ~14% at 6 keV, to only ~3% at 15 keV.

We simulated GPD detected events with polarized and unpolarized X-rays using the GEANT4 package. The effect of diffusion during transportation and multiplication for secondary electrons in the gas chamber was implemented based on simulations with the GARFIELD package. It is two-fold that the simulation is to some extent a good representation of the real measurement: the simulated and measured images are not distinguishable even with trained eyes; the simulated and measured modulations are well consistent with each other within errors [5]. For polarized X-rays, 10^5 events are simulated at each energy. For unpolarized X-rays, 10^6 events are generated in order to see possible systematics of small amplitude.

For each data set, both the old algorithm based on the moment analysis and the new algorithm based on track reconstruction are applied and compared. Their major difference is how to locate the interaction point, upon which step the two algorithms are identical about how to calculate the emission direction from a weighted charge map.

3.1 Distribution of the reconstructed interaction point

The reconstructed interaction points at 15 keV are compared with respect to the known interaction points obtained from simulation for the two algorithms, respectively. Fig. 3 shows the 2D distribution of the reconstructed point around the true point, and Fig. 4 shows the distribution of the distance between them. Compared with the moment analysis based algorithm, the misidentification rate for the new algorithm is much lower and the reconstruction is rather concentrated around the true interaction point. This is particularly remarkable for high energy or complicated tracks. We visually checked the instances of misidentification for both algorithms and found that for the new algorithm almost all of the misidentifications happened for cases where human eyes cannot identify the interaction point, e.g., for looped tracks. On the contrary, the

moment analysis based algorithm often finds the incorrect interaction region as per visual inspection.

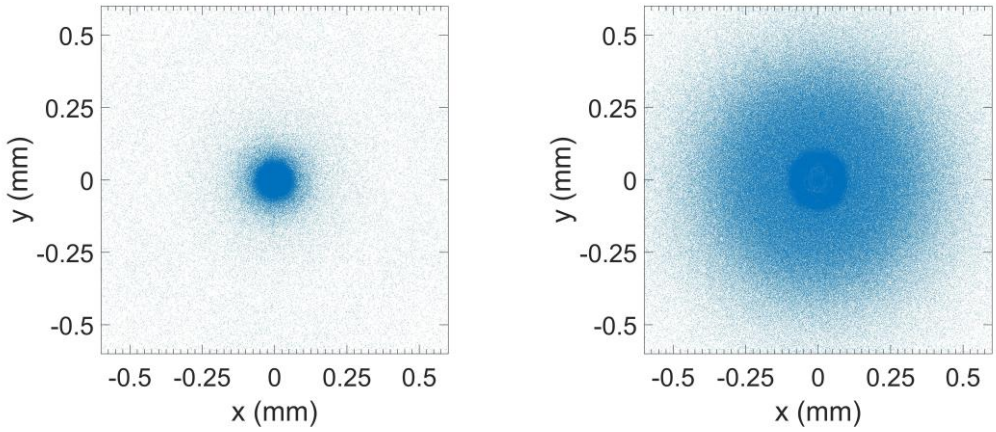

Fig. 3. Distribution of the reconstructed interaction point with respect to the true interaction point (moved to the origin) for the track reconstruction based algorithm (left) and the moment analysis based algorithm (right) for X-rays of 15 keV.

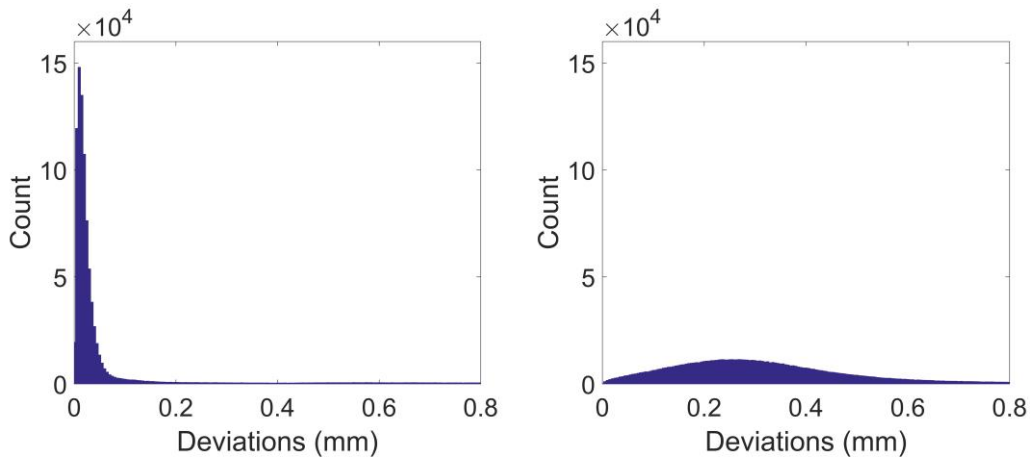

Fig. 4. Distribution of the distance between reconstructed and true interaction points for the track reconstruction based algorithm (left) and the moment analysis based algorithm (right).

3.2 **Modulation factors**

The modulation curves in response to fully polarized X-rays constructed from emission angles based on the new algorithm at different energies from 5 to 15 keV are shown in Fig. 5. They are well consistent with sinusoidal curves. The modulation factors versus energy is shown in Fig. 6 and listed in Table 1. The new algorithm manifests obvious advantage over the old, moment analysis based algorithm. For comparison, the modulation factor calculated with known interaction points from the simulation data are shown in Fig. 6.

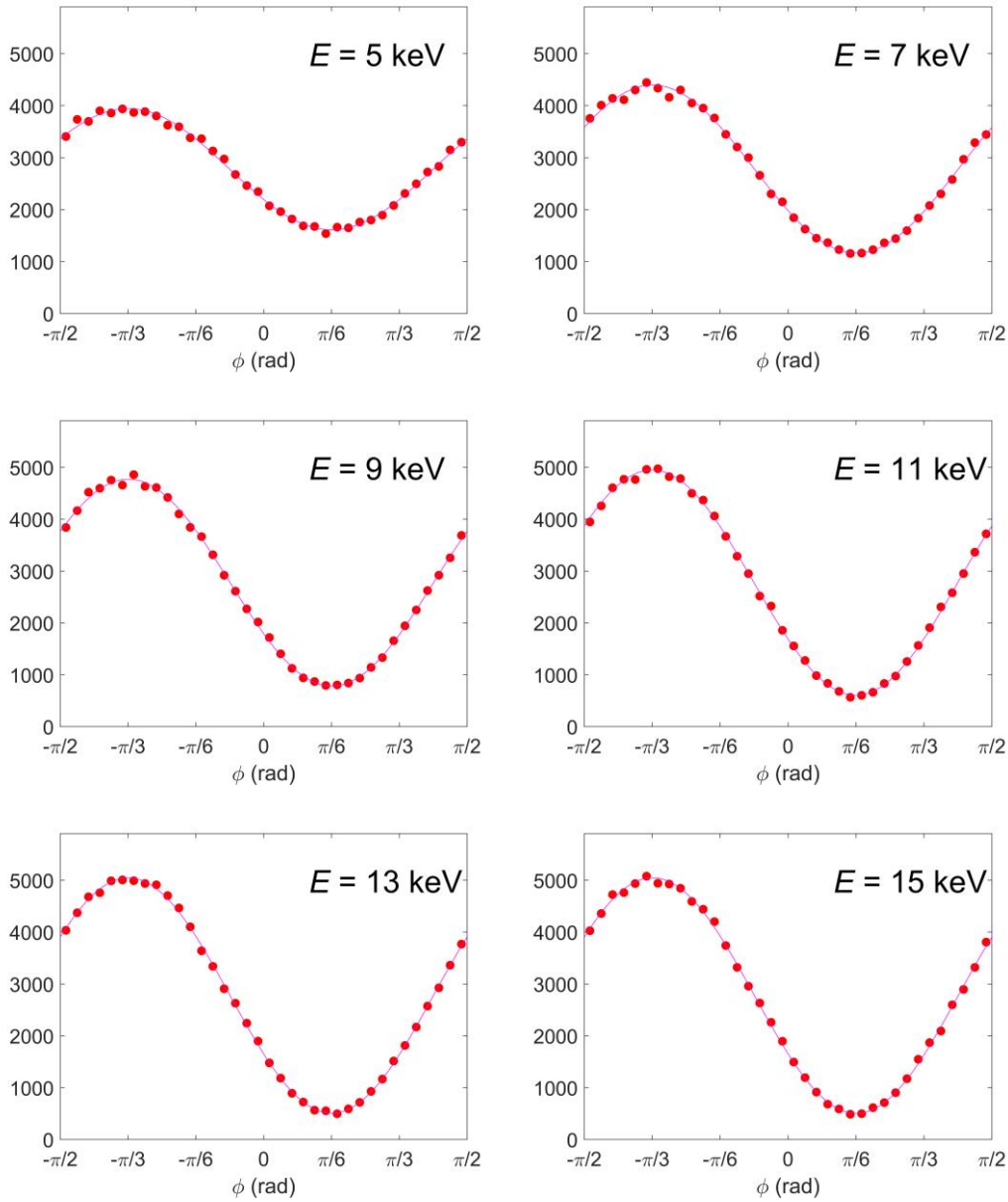

Fig. 5. Modulation curve obtained with the new algorithm at different energies from simulated data. The error bars are smaller than the point.

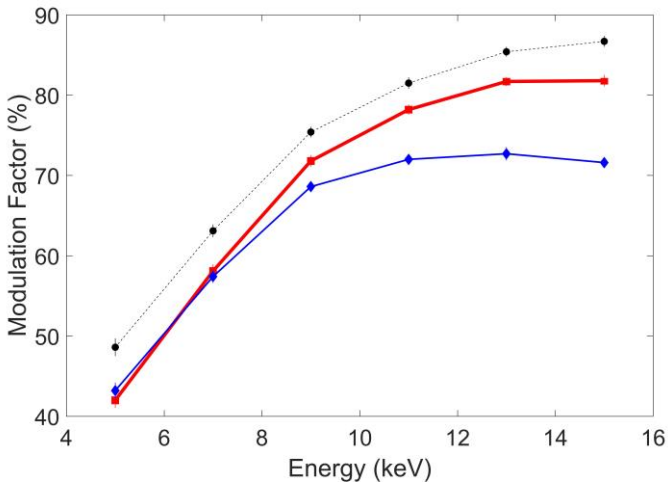

Fig. 6. Modulation factor versus energy derived from the track reconstruction based algorithm (red), the moment analysis based algorithm (blue), and the known interaction points (black).

Table 1. The modulation factor obtained by both algorithms

Energy (E)	5 keV	7 keV	9 keV	11 keV	13 keV	15 keV
μ from track reconstruction (%)	42.0 ± 0.9	58.1 ± 0.8	71.8 ± 0.7	78.2 ± 0.6	81.7 ± 0.6	81.8 ± 0.7
μ from moment analysis (%)	43.2 ± 1.0	57.4 ± 0.8	68.6 ± 0.6	72 ± 0.6	72.7 ± 0.8	71.6 ± 0.6

3.3 **Modulation factors with experimental data**

We also tested the new algorithm with the real measurements, as shown in Fig. 7. The data were adopted from Ref. [5], for fully polarized X-rays at 5.33, 6.09, and 7.49 keV, respectively. To have a direct comparison with those quoted in Ref. [5], we discard 25% of the events with low eccentricity. Results from the measurements are consistent with those from the simulation within errors, as expected. As the measurements are not available at energies above 8 keV, we cannot further test the validity of the algorithm directly for complicated tracks. The good agreement of the simulation and measurement at low energies justifies the use of simulation at high energies.

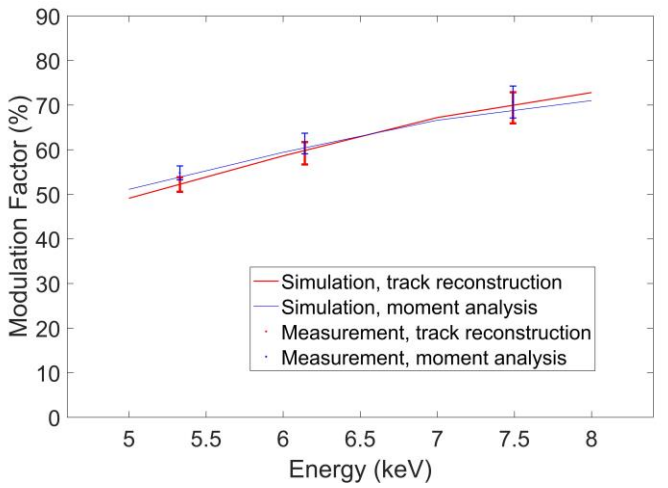

Fig. 7. Comparisons of the modulation factors obtained from both measurements and simulations for both algorithms.

3.4 **Test with unpolarized data**

To test if the new algorithm will produce spurious modulations, we apply it with simulated unpolarized data at 6 and 15 keV, respectively. A million events were generated, corresponding to a minimum detectable modulation of 0.43% at 99% confidence level (a chance of 1% to get a measurement higher than 0.43% given a zero polarized source). Both tests result in a null detection within errors, with a modulation of 0.35% ± 0.31% at 6 keV and 0.15% ± 0.26% at 15 keV. We note that the true distribution of the emission angle for this simulated data set has a modulation of 0.11% ± 0.27% at 6 keV and 0.09% ± 0.30% at 15 keV. Thus, the new algorithm does not introduce detectable systematics.

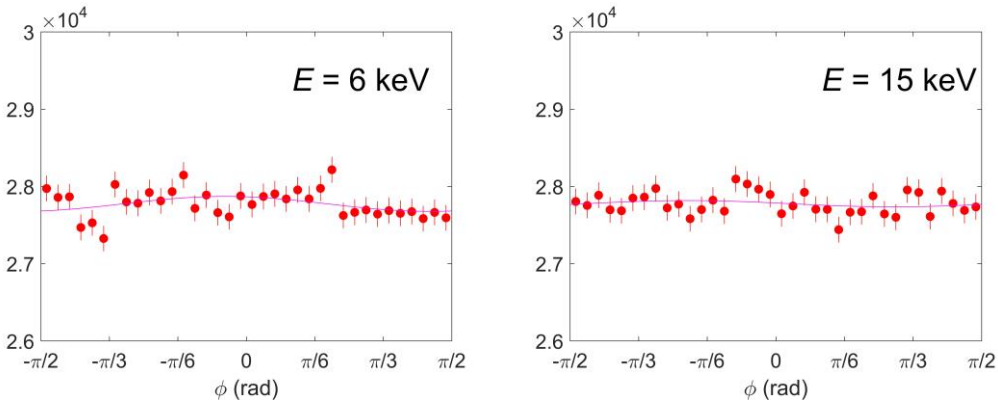

Fig. 8. Modulation curves and best-fit $\cos^2$ functions for unpolarized X-rays at 6 keV and 15 keV. The residual modulation is found to be 0.35% ± 0.31% at 6 keV and 0.15% ± 0.26% at 15 keV, respectively.

4 Conclusion

In this paper, we propose a new algorithm that allows us to reconstruct the 2D photoelectron track in the gas chamber produced by ionization with the electron following the absorption of an X-ray. Compared with previous algorithms that are based on moment analysis, this algorithm is more effective and robust to complicated tracks resulted from high energy photons or low pressure chambers. It can help locate the photoelectric interaction point more accurately (less misidentification) and precisely (smaller scatter) than previous, and lead to a higher modulation factor or sensitivity. Importantly, the new algorithm does not introduce detectable residual modulation or systematics, which determines the limiting sensitivity of the detector.

For the emission angle estimate, we still adopt the previous method that calculates the second moment of a weighted map around the interaction point. In principle, the emission angle can be obtained directly from the reconstructed path. We have tried various methods but all resulted in spurious modulations (deviated from a sinusoidal curve). This should be further investigated in the future.

Acknowledgements

This work was supported by the National Natural Science Foundation of China under grants

11305093 and 11633003, the Tsinghua University Initiative Scientific Research Program (No. 2014Z21016 and 20131089244), and the National Program on Key Research and Development Project (Grant No. 2016YFA040080X).

References:

[1]. Bellazzini, R., et al., Photoelectric X-ray Polarimetry with Gas Pixel Detectors. Nuclear Instruments and Methods in Physics Research Section A: Accelerators, Spectrometers, Detectors and Associated Equipment, 2013. 720: p. 173-177.

[2]. Black, J.K., et al., X-ray polarimetry with a micropattern TPC. Nuclear Instruments and Methods in Physics Research Section A: Accelerators, Spectrometers, Detectors and Associated Equipment, 2007. 581(3): p. 755-760.

[3]. Bellazzini, R., et al., A novel gaseus X-ray polarimeter: data analysis and simulation, in SPIE, S. Fineschi, S. Fineschi^Editors. 2003. p. 383-393.

[4]. Muleri, F., Expectations and perspectives of X-ray photoelectric polarimetry. 2009.

[5]. Li, H., et al., Assembly and test of the gas pixel detector for X-ray polarimetry. 2015.

[6]. Dijkstra, E.W., A note on two problems in connexion with graphs. Numerische Mathematik, 1959. 1(1): p. 269-271.